Estimation of soil moisture from UAS platforms using RGB and thermal imaging sensors in arid and semi-arid regions

P. Paridad[1], S.F. Dal Sasso[1,a], A. Pizarro[1], L. Mita[1], M. Fiorentino[1], M.R. Margiotta[2], F. Faridani[1,3], A. Farid[4] and S. Manfreda[5]

[1]DiCEM, University of Basilicata, Matera, Italy; [2]SI, University of Basilicata, Matera, Italy; [3]CNR-IMAA, Tito, Italy; [4]Department of Water Engineering, Ferdowsi University of Mashhad, Mashhad, Iran; [5]DICEA, University of Naples Federico II, Napoli, Italy.

Abstract

Soil moisture (SM) is a connective hydrological variable between the Earth's surface and atmosphere and affects various climatological processes. Surface soil moisture (SSM) is a key component for addressing energy and water exchanges and can be estimated using different techniques, such as in situ and remote sensing (RS) measurements. Discrete, costly and prolonged, in situ measurements are rarely capable in demonstration of moisture fluctuations. On the other hand, current high spatial resolution satellite sensors lack the spectral resolution required for many quantitative RS applications, which is critical for heterogeneous covers. RS-based unmanned aerial systems (UASs) represent an option to fill the gap between these techniques, providing low-cost approaches to meet the critical requirements of spatial, spectral and temporal resolutions. In the present study, SM was estimated through a UAS equipped with a thermal imaging sensor. To this aim, in October 2018, two airborne campaigns during day and night were carried out with the thermal sensor for the estimation of the apparent thermal inertia (ATI) over an agricultural field in Iran. Simultaneously, SM measurements were obtained in 40 sample points in the different parts of the study area. Results showed a good correlation (R^2=0.81) between the estimated and observed SM in the field. This study demonstrates the potential of UASs in providing high-resolution thermal imagery with the aim to monitor SM over bare and scarcely vegetated soils. A case study based in a wide agricultural field in Iran was considered, where SM monitoring is even more critical due to the arid and semi-arid climate, the lack of adequate SM measuring stations, and the poor quality of the available data.

Keywords: Albedo, bare soil, remote sensing, thermal inertia, vegetation

INTRODUCTION

Soil water content is one of the most essential environmental variables due to its key role in water and energy balances at the land-atmosphere interface (Lu et al., 2018). Surface soil moisture (SSM) is highly varied in space and time and across different scales; therefore, detailed information on soil water content is of practical importance, especially over arid and semi-arid regions, which aims at improving water resources utilization efficiency, food productivity, irrigation planning and achieving sustainable water resources management (Engman, 1991; Bolten et al., 2010; Robinson et al., 2008).

Direct in situ observations of SSM are prolonged, labor-intensive, costly, and limited to discrete measurements in point scale, which precludes the spatial distribution of SSM due to its temporal and spatial variability (Crow et al., 2012). An alternative to measure and monitor large-scale SSM is the application of remotely-sensed (RS) products (Wang and Qu, 2009). Soil surface reflectance is the basis of SM monitoring through visible radiation methods, while thermal infrared radiation (TIR) methods function on the sensitivity of land surface

[a]E-mail: silvano.dalsasso@unibas.it

temperature (LST) to SSM (Petropoulos et al., 2015). RS methods based on microwave radiation functions relied on the high level of difference between the soil and water dielectric constants (Jackson, 1993).

SM estimations at coarse spatial resolution have been provided from several satellite missions including soil moisture and ocean salinity (SMOS) (Kerr et al., 2001), soil moisture active and passive (SMAP) (Entekhabi et al., 2010), and advanced scatterometer (ASCAT) (Wagner et al., 2013). However, SM spatial-temporal variability (Brocca et al., 2010) creates challenges in accurately estimating soil water content even through the current high-resolution satellite sensors and despite the recent advances in RS methods (El Hajj et al., 2017; Kim and Lakshmi, 2018).

In the last decade, with the increasing developments in Unmanned Aerial Systems (UASs), they have been promoted as a suitable alternative for precise monitoring due to their high versatility, flexibility, and the ability to operate rapidly without necessarily planned scheduling. UASs represent major advantages against conventional platforms that have been broadly used over the years due to the ability to acquire near real-time ultra-high spatial and temporal resolution aerial maps with low operational costs (Pajares, 2015; Manfreda et al., 2018; Tmusic et al., 2020).

Rapid signs of progress in the use of TIR techniques for soil moisture investigations have been made since 1974 (Pratt and Ellyett, 1979). The thermal RS methods estimate SM based on soil thermal properties or LST measurements at the TIR wavelengths (3 to 14 μm). Vegetation indices affected by climate conditions are included in the latter empirical methods (Lu et al., 2018). However, the former approach relates SM to soil Thermal Inertia (TI), an intrinsic property that represents the ability of surface soil to resist temperature change. High TI values indicate small changes in temperature, while the reverse is true for low TI values (Pratt and Ellyett, 1979). Heat capacity and thermal conductivity as the two elements governing the TI, increase as SM increases; thus, SM can be inversely determined using TI if a relationship between these parameters is obtained in advance (Matsushima et al., 2011).

An algorithm was first developed by (Price, 1980, 1985) to measure TI through satellite measurements of surface temperature by deriving an analytical expression that illustrates the satellite-based retrieved relation between bare soil temperature, mean evaporation and TI. Due to the requirements of a large number of observed ground data for model calibration in the TI-based empirical equations proposed by (Verstraeten et al., 2006; Matsushima et al., 2011), these approaches are unavailable for many regions. Soil texture and porosity have been applied in models that relate TI to SM by Minacapilli et al. (2012), Lu et al. (2018), Paruta et al. (2020).

Only a few studies have monitored SM through RS in Iran despite the importance of water in this arid and semi-arid region (Rahmani et al., 2016; Fakharizadehshirazi et al., 2019; Gheybi et al., 2019); on the other hand, the thermal inertia approach for SM estimation and UAS application have never been tested in this region. The present study gives a description on generating high-resolution SM products through applying a TI approach in this poorly monitored area by the application of drone-based thermal imagery.

MATERIALS AND METHODS

Study area

The experimental site, selected for the execution of field and aerial surveys, was located 10 km from the Municipality of Neishabour, Iran (Figure 1), which comprises a total area of 2 ha. From the climatic point of view, the territory is part of the Eutemperate region with the biotope of the semi-desert. The annual average precipitation and potential evapotranspiration in this basin are 247.4 and 2335 mm, respectively. The highest and lowest monthly-averaged precipitations fall in March and August with values of 51 and 0.16 mm, respectively. The land use is characterized by bare soils and heterogeneous low vegetated agricultural fields. The main type of crop occurring at the aerial imagery acquisition day was wheat; although, some parts of the area were irrigated for saffron cultivation.

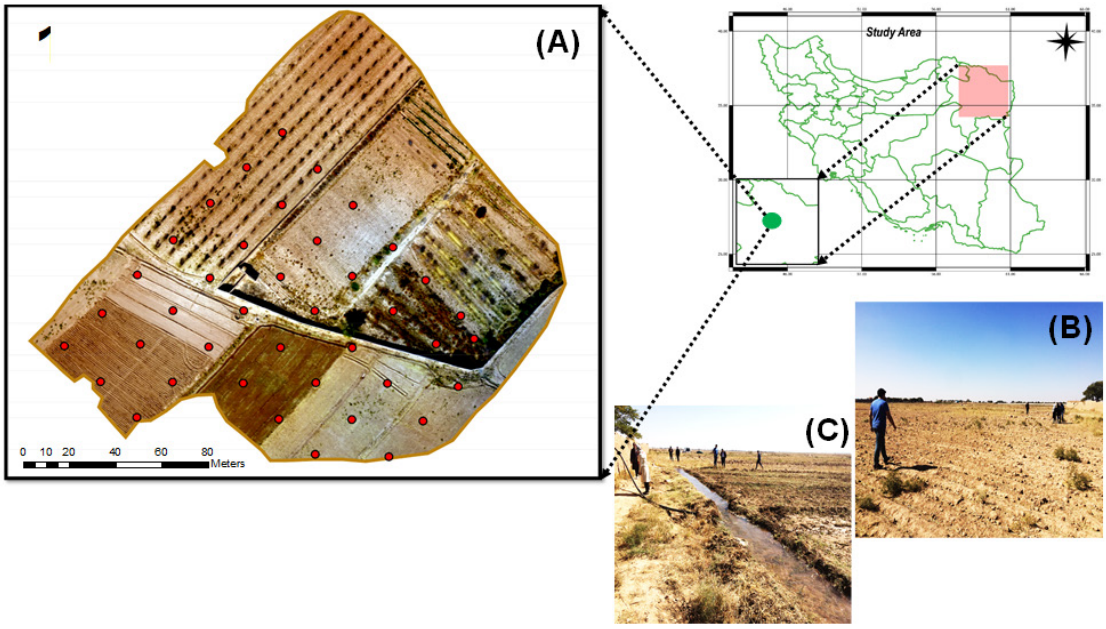

Figure 1. Location of the study area (A) Triband orthomosaic over study site overlapped with observed SM data (red symbols), (B) and (C) Field survey performed on 17 October 2018.

Thermal data

On 17 October 2018, two flight campaigns were carried out over the study area with a FLIR Tau2 336 thermal sensor (FLIR Systems, Inc. Wilsonville, Oregon, USA) installed onboard a quadcopter DJI Phantom 3 Pro (SZ DJI Technology Co., Ltd. Shenzhen, Guangdong, China), which was equipped with an RGB color filter array camera of FC 300X.

The first aerial survey was carried out around 11:30 in the morning UTC in order to evaluate the daily increase in surface soil temperature, while the second one was conducted on the same day at 20:00 UTC to estimate the soil temperature in the absence of solar load. Both surveys were performed in clear sky conditions. Flight height was set according to a ground sampling distance (GSD) of 19 and 4.6 cm for thermal and RGB images, respectively, and the flight plan applied a cross pattern with 90% side lap and 90% forward overlap. The radiometric solution produces thermographic IR video files in ".TMC" format, which were visualized, processed, and radiometrically corrected with ThermoViewer Software to extract 426 and 476 thermal images during day and nighttime, respectively. The procedure of georeferencing the thermal images was conducted in Geosetter Software in order to assign geographical data to each image metadata, and the final thermal orthomosaics were obtained in Pix4D Mapper Software. Afterward, ground control points (GCPs) obtained on the field were assigned to the thermal and RGB orthomosaics to ensure a proper overlap. A total of 184 RGB images were acquired to build the triband orthomosaic (Figure 1), which was further applied to extract the normalized green red difference index (NGRDI).

In situ data

Simultaneously with the acquisition of the thermal images, a ground campaign was carried out to collect soil samples at 40 locations. The sampling was carried out on bare soil, which were further analyzed using the method of hydrometer in the laboratory to obtain the amount of each particle fraction from the United States Department of Agriculture (USDA) soil texture triangle. In particular, SM in 40 points was measured at a depth of 10-15 cm from a FieldScout TDR300 Soil Moisture Meter (by Spectrum Technologies, Inc.), which was applied to measure soil volumetric water content and were further analyzed in the validation

procedures of the SM map. This portable device consists of a probe with 0.15 m long steel rods and is characterized by a soil moisture resolution of 0.1%. Table 1 shows the characteristics of the observed SM data.

Table 1. Soil moisture of soil samples collected on 17 October 2018.

Soil sample	Latitude (°N)	Longitude (°E)	Soil moisture (%)	Soil sample	Latitude (°N)	Longitude (°E)	Soil moisture (%)
1	36°8'9.76"	58°51'39.10"	10.4	21	36°8'11.23"	58°51'35.19"	8.4
2	36°8'10.23"	58°51'38.55"	4.4	22	36°8'11.68"	58°51'35.78"	8.3
3	36°8'10.70"	58°51'38.00"	3.1	23	36°8'10.81"	58°51'33.48"	5.8
4	36°8'11.18"	58°51'37.45"	4.6	24	36°8'10.37"	58°51'32.89"	5.7
5	36°8'11.65"	58°51'36.90"	5.5	25	36°8'9.93"	58°51'32.31"	5.6
6	36°8'11.20"	58°51'36.32"	5.6	26	36°8'9.3"	58°51'32.86"	6
7	36°8'10.74"	58°51'36.87"	6.5	27	36°8'9.8"	58°51'33.44"	5.4
8	36°8'10.26"	58°51'37.42"	8.3	28	36°8'10.35"	58°51'34.03"	6.6
9	36°8'9.79"	58°51'37.97"	6.8	29	36°8'10.32"	58°51'35.16"	8
10	36°8'9.32"	58°51'38.52"	11.6	30	36°8'9.87"	58°51'34.58"	8.3
11	36°8'9.35"	58°51'37.39"	13.6	31	36°8'9.42"	58°51'33.99"	5.5
12	36°8'9.82"	58°51'36.84"	22.2	32	36°8'8.98"	58°51'33.41"	6.1
13	36°8'10.29"	58°51'36.29"	5.2	33	36°8'8.95"	58°51'34.54"	50.3
14	36°8'10.76"	58°51'35.74"	5.2	34	36°8'9.39"	58°51'35.12"	51.4
15	36°8'12.12"	58°51'36.35"	5.8	35	36°8'8.92"	58°51'35.67"	55.2
16	36°8'12.60"	58°51'35.81"	7.2	36	36°8'8.49"	58°51'35.10"	57.1
17	36°8'12.16"	58°51'35.23"	7.1	37	36°8'8.45"	58°51'36.22"	11.3
18	36°8'11.71"	58°51'34.64"	8.1	38	36°8'8.43"	58°51'37.36"	9.6
19	36°8'11.27"	58°51'34.07"	7.6	39	36°8'8.90"	58°51'36.81"	12.3
20	36°8'10.79"	58°51'34.61"	7.8	40	36°8'8.87"	58°51'37.94"	12.1

Thermal inertia and soil moisture

The temperature of the soil's surface is influenced by many physical parameters, and the trends in temperature fluctuations of soil depend on its different thermal properties (Cheruy et al., 2017). The method applied in this study is to derive SM distribution based on TI, which describes the impedance of soil to temperature variations (Kahle et al., 1976). TI (J m^{-2} K^{-1} $s^{-1/2}$) is determined by volumetric heat capacity (c, J m^{-3} K^{-1}) and thermal conductivity (k, W m^{-1} K^{-1}) of the surface layer:

$$TI = \sqrt{c \times k} \quad (1)$$

Variations in temperature that occur during a diurnal solar cycle are caused by variations of TI. High TI indicates a high resistance to temperature change, resulting in a low difference in temperature (e.g., wet soils). The opposite happens to surfaces characterized by low TI (e.g., dry soils). Therefore, SM can be estimated from the differences in soil temperatures during the day (Price, 1980). TI cannot be derived directly due to dependency on factors that cannot be retrieved from remote observations (c and k can only be measured in situ); therefore, (Price, 1985) simplified the estimation of TI through application of apparent thermal inertia (ATI).

$$ATI = 1 - \alpha/\Delta T \quad (2)$$

where α is the surface albedo and ΔT (K) is the difference between the maximum and minimum soil surface temperatures during a diurnal solar cycle.

The procedure followed, as shown in Figure 2, included the derivation of ATI map using the FLIR Tau2 sensor (for diurnal ΔT estimation) and the grayscale reflection map from RGB sensor (for albedo estimation). In order obtain a good relationship between ATI and SM, the TI method must be applied over bare or scarcely vegetated soils (Jackson, 1993); therefore,

the RGB orthomosaic was firstly applied to create a mask of bare soils and separate the vegetated pixels using the NGRDI index (Yang, 2018). The common range for green vegetation is 0.1-0.8. The NGRDI threshold for separation of green vegetation from bare soils in the selected study area was 0.15. Once removing the vegetated pixels from the thermal map, it is necessary also to remove the shadow of vegetation. In this regard, while investigating the histogram of the ATI map masked by NGRDI index, a bi-modal distribution was observed. The first peak with lower temperature values characterizes the shadowed pixels and the second peak with higher temperatures corresponds to wet and dry soil pixels. The minimum between these two peaks was chosen as a threshold to remove the vegetated pixels. ATI is dependent on boundary conditions; therefore, a normalization analogous has to be performed (Minacapilli et al., 2012):

$$K_{ATI} = \frac{ATI - ATI_{dry}}{ATI_{sat} - ATI_{dry}} \quad (3)$$

where ATI_{dry} (K^{-1}) is ATI of dry soils, and ATI_{sat} (K^{-1}) represents the ATI of saturated soils, which are the minimum and maximum values of ATI spatial distributions during a time series, respectively. Considering the normalized value of ATI and soil porosity, the SM spatial distribution was derived from the equation below.

$$\theta = \Phi \left[1 - \frac{\ln K_{ATI}}{\varepsilon}\right]^{(1/-\mu)} \quad (4)$$

where Φ is the soil porosity, ε and μ are two empirical parameters equal to 0.6 and 0.71 for fine-textured soils, respectively, whereas for coarse-textured soils these values are 2.95 and 0.16, respectively (Minacapilli et al., 2012).

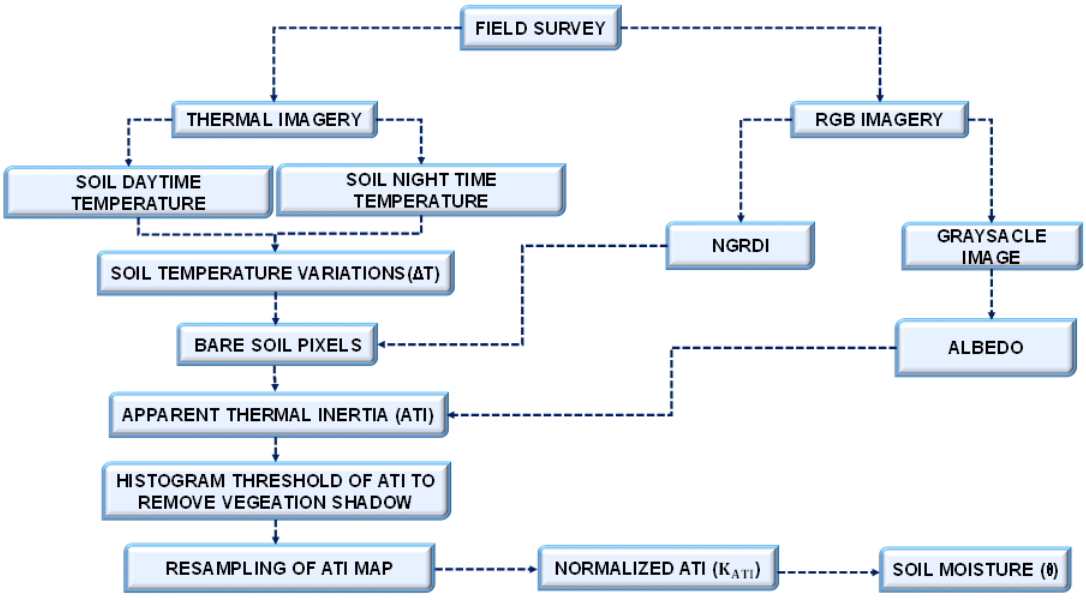

Figure 2. Flowchart of the applied methodology.

RESULTS AND DISCUSSION

In this study, the spatial distribution of SM was derived through a remotely sensed ATI map. In the following sections, we present the temperature, ATI, and SM maps.

Temperature and ATI maps

Two temperature maps were obtained from the FLIR Tau2 sensor after the stitching and

radiometrically correction of the imageries. The retrieved temperature maps are shown in Figure 3. In particular, Figure 3A shows the temperature map of the morning flight, ranging from 287 to 332 K; while, the temperature map of the nighttime flight, which varies between 273 and 286 K is shown in Figure 3B. Cai et al. (2007) illustrated that a temperature variation of the order of 10 K is sufficient for an accurate estimation of SM, which is in concordance with the obtained temperature range.

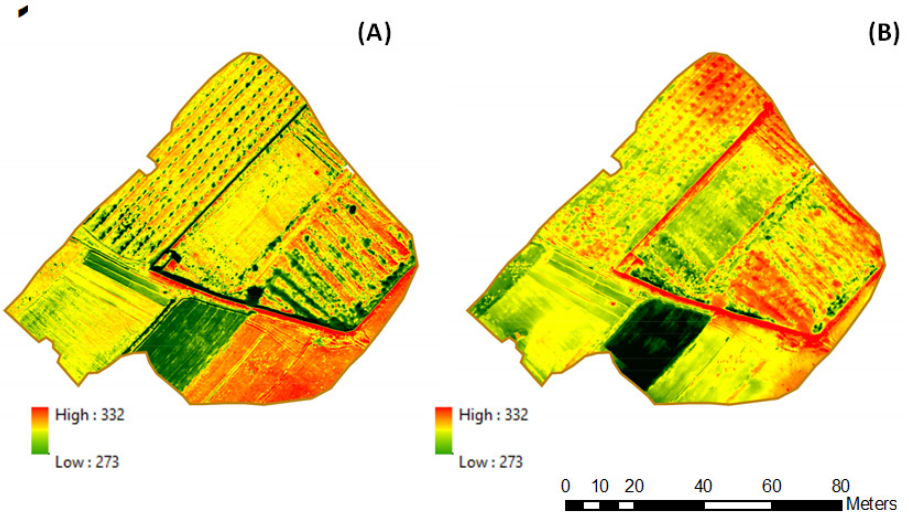

Figure 3. Soil surface temperatures obtained from the thermal camera (A) during maximum solar load; (B) at night.

The ATI map obtained from the temperature variations of the study field after separating the vegetation and its shadow is illustrated in Figure 4A. After this step, a resampling method was applied over the ATI map to perform an averaging of 1 m over the pixels due to the ultra-high resolution of pixels.

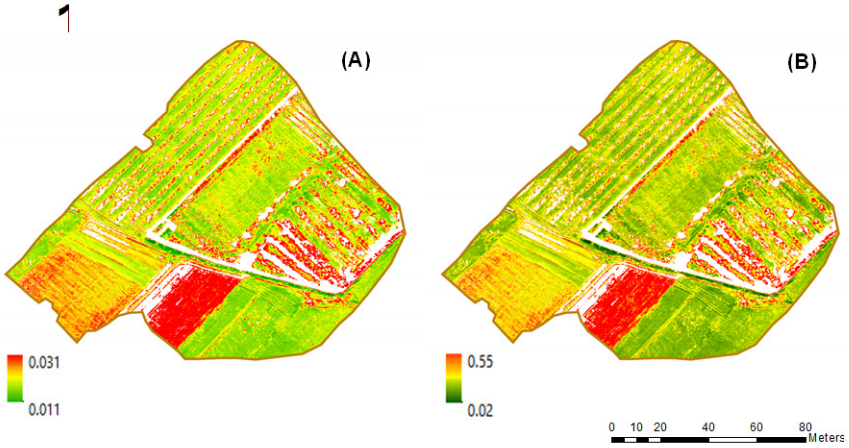

Figure 4. (A) ATI map of the bare soils of the study area. The ATI values in the map are expressed in K^{-1} units; (B) Map of SM derived from FLIR thermal camera onboard the UAS expressed in $m^3 m^{-3}$.

Soil moisture map

The laboratory analyses' results of the collected soil samples in the study area

highlighted that all of our samples are almost homogeneous in terms of texture and recommended clay loam as the main soil texture in different parts of the field; thus, the parameters of Φ, ε, and μ were considered equal to 0.50, 0.6 and 0.71, respectively (Minacapilli et al., 2012). SM spatial distribution corresponding to the 40 sample points was obtained by using Equation (4). Calculated SM values were compared with the measured ones (Figure 5A). The R^2=0.81 and RMSE=0.03 were obtained, which are in full agreement with (Palombo et al., 2019).

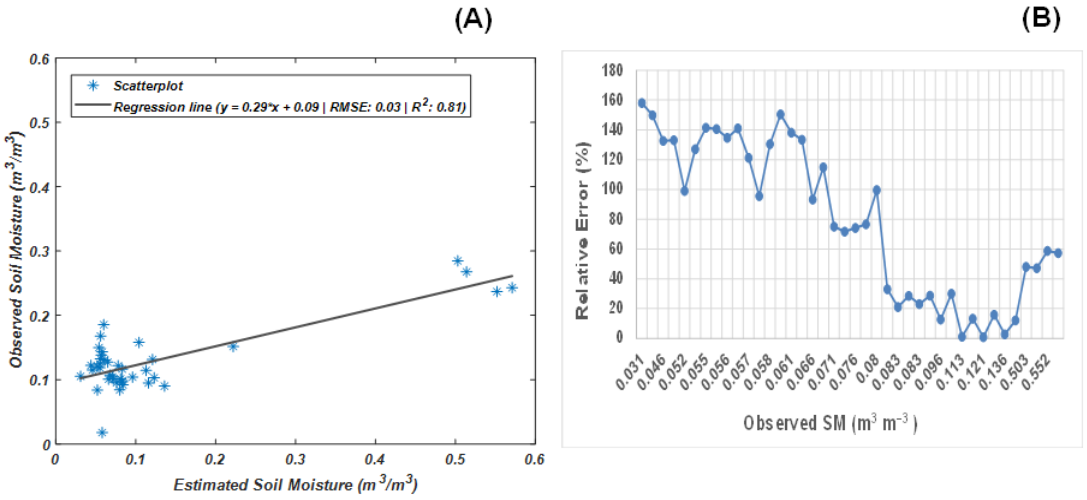

Figure 5. (A) Scatterplot of estimated vs. observed SM; (B) Relative errors observed in each sample point vs. the observed SM values.

Other studies have also demonstrated a good relationship between ATI over bare soils and SM values, as verified in our research (Verstraeten et al., 2006; Minacapilli et al., 2012). Visual examination of SM (Figure 4B) indicates spatial trends of soil water content for bare and low vegetated soils in the study area, including observation of the lowest SM values identified in the northwest side of the acquired imagery; while, high SM values were recognized along the central section of the study area that is characterized by the irrigation performed for saffron cultivation.

As shown in Figure 5B, the TI method applied on the thermal imagery obtained from the UAS estimated SM accurately in the medium range of its values from 8 up to 30% and showed the minimum relative error ($100\times|measured\ SM - observed\ SM|)/observed\ SM$) values up to 30%. However, in the southwestern part of the field covered with the driest soils with less than 8% of water content, and in the middle-irrigated zone that water content was recorded by TDR up to 50%, this method was not able to estimate the SM values very precisely, and the errors obtained from the model results show higher error values. Based on similar results obtained by (Minacapilli et al., 2012), it can be concluded that the applied method overestimated the values corresponding to soil water contents <0.05 $m^3\ m^{-3}$. The errors observed in value ranges higher than 30% could be due to a different porosity value over this zone, which will affect the SM results greatly since one porosity value for all parts of the field was applied. Another possible source of underestimations in this zone lies in the albedo calculations. Due to lack of multispectral sensor onboard the UAS, the albedo map was obtained from the grayscale reflection imagery and by comparing the maximum reflection amount from a total white pixel with the value of 255 with all the desired pixels throughout the field and by considering the known albedo value of the white surface. The albedo values over the irrigated area are lower than the dry soil due to lower reflections from the wet surface. Since the albedo calculation procedure was not from a multispectral camera, the albedo values over the irrigated area and the driest part of the field were overestimated, which affected the final SM results. Moreover, it should be considered that in the process of extracting

vegetation from bare soil pixels, there were some vegetated pixels that were not precisely extracted due to the fact that separating 100% pixels of vegetation is nearly impossible since the resolution of thermal and RGB sensors are different. More importantly, we applied an RGB index instead of the most commonly used NDVI to separate vegetation from soil, which distinguishes vegetation from soil so much better. Therefore, by applying an RGB index, separating the exact pixels of vegetation from soil cannot be done due to the almost similar reflection from red, greed, and blue bands rather than NIR, which is applied in NDVI. Consequently, applying a multispectral sensor and calculating NDVI is suggested in future studies.

CONCLUSIONS

In this study, a TI approach was applied to retrieve SM for bare and scarcely vegetated soils by integrating high spatial resolution thermal imagery onboard a UAS regarding the fact that diurnal thermal behavior of soil surface temperature is affected by fluctuations in SSM. For this purpose, ground soil sampling was carried out in the study area in order to determine the top soil moisture content and the composition of the soil samples. These data were used to validate the SM obtained on the basis of two different airborne thermal surveys. The results obtained with an R^2=0.81 show a satisfactory relation between in situ observations and the estimated SM values obtained from integration of soil texture properties and surface temperature with an accuracy that can be considered satisfactory for practical purposes. The potential of UASs in acquiring high-resolution thermal data was evaluated in this study, suggesting that these instruments represent a fast, reliable, and cost-effective resource in measuring crop biophysical variables in precision farming applications as well as soil water content as an aid for sustainable water management in the agricultural domain over arid and semi-arid regions. The authors are currently working with a larger data set, including a wider range of soil moisture conditions, to generalize this methodology.

ACKNOWLEDGEMENTS

This project was funded by the Cooperation Project “Pietro della Valle” entitled “Monitoraggio dello stato di imbibizione dei suoli in ambienti semiaridi” funded by CRUI, 2017 Pietro della Valle.

Literature cited

Bolten, J.D., Crow, W.T., Zhan, X., Jackson, T.J., and Reynolds, C.A. (2010). Evaluating the utility of remotely sensed soil moisture retrievals for operational agricultural drought monitoring. IEEE J-STARS *3* (*1*), 57–66 https://doi.org/10.1109/JSTARS.2009.2037163.

Brocca, L., Melone, F., Moramarco, T., and Morbidelli, R. (2010). Spatial-temporal variability of soil moisture and its estimation across scales. Water Resour. Res. *46* (*2*), https://doi.org/10.1029/2009WR008016.

Cai, G., Xue, Y., Hu, Y., Wang, Y., Guo, J., Luo, Y., Wu, C., Zhong, S., and Qi, S. (2007). Soil moisture retrieval from MODIS data in Northern China Plain using thermal inertia model. Int. J. Remote Sens. *28* (*16*), 3567–3581 https://doi.org/10.1080/01431160601034886.

Cheruy, F., Dufresne, J.L., Mesbah, S.A., Grandpeix, J.Y., and Wang, F. (2017). Role of soil thermal inertia in surface temperature and soil moisture-temperature Feedback. J. Adv. Model. Earth. Sy. *9*, 2906–2919.

Crow, W., Berg, A., Cosh, M.H., Loew, A., Mohanty, B.P., Panciera, R., de Rosnay, P., Ryu, D., and Walker, J. (2012). Upscaling sparse ground-based soil moisture observations for the validation of coarse-resolution satellite soil moisture products. Rev. Geophys. *50* (*2*), 1–20 https://doi.org/10.1029/2011RG000372.

El Hajj, M., Baghdadi, N., Zribi, M., and Bazzi, H. (2017). Synergic use of sentinel-1 and sentinel-2 images for operational soil moisture mapping at high spatial resolution over agricultural areas. Remote Sens. *9* (*12*), 1292 https://doi.org/10.3390/rs9121292.

Engman, E.T. (1991). Applications of microwave remote sensing of soil moisture for water resources and agriculture. Remote Sens. Environ. *35* (*2-3*), 213–226 https://doi.org/10.1016/0034-4257(91)90013-V.

Entekhabi, D., Njoku, E.G., O’Neill, P.E., Kellogg, K.H., Crow, W.T., Edelstein, W.N., Entin, J.K., Goodman, S.D., Jackson, T.J., Johnson, J., et al. (2010). The soil moisture active passive (SMAP). Mission. Proc. IEEE *98* (*5*), 704–716 https://doi.org/10.1109/JPROC.2010.2043918.

Fakharizadehshirazi, E., Sabziparvar, A.A., and Sodoudi, S. (2019). Long-term spatiotemporal variations in satellite-based soil moisture and vegetation indices over Iran. Environ. Earth Sci. *78* (*12*), 342 https://doi.org/10.1007/s12665-019-8347-4.

Gheybi, F., Paridad, P., Faridani, F., Farid, A., Pizarro, A., Fiorentino, M., and Manfreda, S. (2019). Soil moisture monitoring in Iran by implementing satellite data into the root-zone SMAR model. Hydrology *6* (*2*), 44 https://doi.org/10.3390/hydrology6020044.

Jackson, T.J. (1993). III. Measuring surface soil moisture using passive microwave remote sensing. Hydrol. Processes *7* (*2*), 139–152 https://doi.org/10.1002/hyp.3360070205.

Kahle, A.B., Gillespie, A.R., and Goetz, A.F.H. (1976). Thermal inertia imaging: a new geologic mapping tool. Geophys. Res. Lett. *3* (*1*), 26–28 https://doi.org/10.1029/GL003i001p00026.

Kerr, Y.H., Waldteufel, P., Wigneron, J., Martinuzzi, J., Font, J., and Berger, M. (2001). Soil moisture retrieval from space: the Soil Moisture and Ocean Salinity (SMOS) mission. IEEE Trans. Geosci. Remote Sens. *39* (*8*), 1729–1735 https://doi.org/10.1109/36.942551.

Kim, H., and Lakshmi, V. (2018). Use of Cyclone global navigation satellite system (CyGNSS) observations for estimation of soil moisture. Geophys. Res. Lett. *45* (*16*), 8272–8282 https://doi.org/10.1029/2018GL078923.

Lu, Y., Horton, R., Zhang, X., and Ren, T. (2018). Accounting for soil porosity improves a thermal inertia model for estimating surface soil water content. Remote Sens. Environ. *212*, 79–89 https://doi.org/10.1016/j.rse.2018.04.045.

Manfreda, S., McCabe, M.F., Miller, P.E., Lucas, R., Pajuelo Madrigal, V., Mallinis, G., Ben-Dor, E., Helman, D., Estes, L., Ciraolo, G., et al. (2018). On the use of unmanned aerial systems for environmental monitoring. Remote Sens. *10* (*4*), 641 https://doi.org/10.3390/rs10040641.

Matsushima, D., Kimura, R., and Shinoda, M. (2011). Soil moisture estimation using thermal inertia: potential and sensitivity to data conditions. J. Hydrometeorol. *13* (*2*), 638–648 https://doi.org/10.1175/JHM-D-10-05024.1.

Minacapilli, M., Cammalleri, C., Ciraolo, G., D'Asaro, F., Iovino, M., and Maltese, A. (2012). Thermal inertia modeling for soil surface water content estimation: a laboratory experiment. Soil Sci. Soc. Am. J. *76* (*1*), 92–100 https://doi.org/10.2136/sssaj2011.0122.

Pajares, G. (2015). Overview and current status of remote sensing applications based on unmanned aerial vehicles (UAVs). Photogramm. Eng. Rem. S *81*, 281–330 https://doi.org/10.14358/pers.81.4.281.

Palombo, A., Pascucci, S., Loperte, A., Lettino, A., Castaldi, F., Muolo, M.R., and Santini, F. (2019). Soil moisture retrieval by integrating TASI-600 airborne thermal data, worldview 2 satellite data and field measurements: Petacciato Case Study. Sensors (Basel) *19* (*7*), 1515 https://doi.org/10.3390/s19071515. PubMed

Paruta, A., Nasta, P., Ciraolo, G., Capodici, F., Manfreda, S., Romano, N., Bendor, E., Zeng, Y., Maltese, A., Dal Sasso, S.F., and Zhuang, R. (2020). A geostatistical approach to map near-surface soil moisture through hyper-spatial resolution thermal inertia. IEEE Trans. Geosci. Remote Sens. https://doi.org/10.1109/TGRS.2020.3019200.

Petropoulos, G.P., Ireland, G., and Barrett, B. (2015). Surface soil moisture retrievals from remote sensing: current status, products & future trends. Phys. Chem. Earth Parts ABC *83–84*, 36–56 https://doi.org/10.1016/j.pce.2015.02.009.

Pratt, D.A., and Ellyett, C.D. (1979). The thermal inertia approach to mapping of soil moisture and geology. Remote Sens. Environ. *8* (*2*), 151–168 https://doi.org/10.1016/0034-4257(79)90014-2.

Price, J.C. (1980). The potential of remotely sensed thermal infrared data to infer surface soil moisture and evaporation. Water Resour. Res. *16* (*4*), 787–795 https://doi.org/10.1029/WR016i004p00787.

Price, J.C. (1985). On the analysis of thermal infrared imagery: the limited utility of apparent thermal inertia. Remote Sens. Environ. *18* (*1*), 59–73 https://doi.org/10.1016/0034-4257(85)90038-0.

Rahmani, A., Golian, S., and Brocca, L. (2016). Multiyear monitoring of soil moisture over Iran through satellite and reanalysis soil moisture products. Int. J. Appl. Earth Obs. Geoinf. *48*, 85–95 https://doi.org/10.1016/j.jag.2015.06.009.

Robinson, D., Campbell, C., Hopmans, J., Hornbuckle, B., Jones, S., Knight, R., Ogden, F., Selker, J., and Wendroth, O. (2008). Soil moisture measurement for ecological and hydrological watershed-scale observatories: a review. Vadose Zone J. *7* (*1*), 358–389 https://doi.org/10.2136/vzj2007.0143.

Tmušić, G., Manfreda, S., Aasen, H., James, M., Gonçalves, G., Ben-Dor, E., Brook, A., Polinova, M., Arranz, J.J., Mészáros, J., et al. (2020). McCabe, Practical guidance for UAS-based environmental mapping. Remote Sens. *12*, 1001 https://doi.org/10.3390/rs12061001.

Verstraeten, W.W., Veroustraete, F., van der Sande, C.J., Grootaers, I., and Feyen, J. (2006). Soil moisture retrieval using thermal inertia, determined with visible and thermal spaceborne data, validated for European forests.

Remote Sens. Environ. *101* (*3*), 299–314 https://doi.org/10.1016/j.rse.2005.12.016.

Wagner, W., Hahn, S., Kidd, R., Melzer, T., Bartalis, Z., Hasenauer, S., Figa-Saldaña, J., de Rosnay, P., Jann, A., Schneider, S., et al. (2013). The ASCAT soil moisture product: a review of its specifications, validation results, and emerging applications. Meteorol. Z. (Berl.) *22* (*1*), 5–33 https://doi.org/10.1127/0941-2948/2013/0399.

Wang, L., and Qu, J.J. (2009). Satellite remote sensing applications for surface soil moisture monitoring: A review. Front. Earth Sci. China *3* (*2*), 237–247 https://doi.org/10.1007/s11707-009-0023-7.

Yang, D. (2018). Gobi vegetation recognition based on low-altitude photogrammetry images of UAV. IOP Conf. Ser. Earth Environ. Sci. *186*, 012053 https://doi.org/10.1088/1755-1315/186/5/012053.